Magnetoresistance and nanoscopic magnetic coherence in some frustrated ferromagnets

Paolo Allia,[1] Marco Coisson,[2] Javier Moya,[1] Vincenzo Selvaggini,[1] Paola Tiberto,[2] and Franco Vinai[2]
[1]*Dipartimento di Fisica, Politecnico di Torino, and INFM, Research Unit Torino Politecnico, Corso Duca degli Abruzzi 24, I-10129 Torino, Italy*
[2]*Istituto Elettrotecnico Nazionale Galileo Ferraris and INFM, Research Unit Torino Politecnico, Strada delle Cacce 91, I-10135 Torino, Italy*

(Received 28 October 2002; revised manuscript received 21 January 2003; published 19 May 2003)

Measurements of magnetic and magnetotransport properties of frustrated metallic ferromagnets are combined to get information on their equilibrium spin pattern over distances of the order of the nanometer. The considered systems are concentrated, chemically homogeneous solid solutions of one or more transition metals in a host diamagnetic metal; competing interactions produce a significant magnetic frustration and a ultrashort ferromagnetic coherence length over an extended range of temperatures. The isotropic negative magnetoresistance exhibited by these systems is instrumental for obtaining information on changes of the spin pattern on the nanometer scale. Recent magnetic and magnetotransport data obtained on three frustrated ferromagnets ($Au_{80}Fe_{20}$, $Au_{70}Fe_{30}$, and $Cu_{60}Fe_{20}Ni_{20}$) are briefly discussed. The magnetoresistance behavior of these systems is related to the changes of the magnetic coherence length by effect of both temperature and applied magnetic field.

DOI: 10.1103/PhysRevB.67.174412 PACS number(s): 73.63.−b, 72.25.Ba, 75.50.Lk, 75.75.+a

I. INTRODUCTION

Although magnetoresistance (MR) phenomena have been investigated since the very beginning of modern magnetism, renewed interest has occurred since the discovery of giant magnetoresistance (GMR) in magnetic multilayers, which opened the way to a variety of recent applications.[1–3] As a consequence of this application-oriented research activity, other possible outcomes of MR phenomena in unconventional magnetic systems have been somewhat neglected, in spite of their implications at a basic level. Disordered magnetism is a subject in which the potential of MR as a breakthrough technique is still partially unexplored. As a matter of fact, magnetoresistance is intrinsically connected with the electron mean free path (mfp),[2,4] i.e., with a range of distances of the order of a few nanometers in most disordered metallic alloys at room temperature. This feature is key for understanding the usefulness of MR in determining the properties of almost all last-generation magnetic materials, where nanoscopic lengths or volumes and related nanoscale properties play a major role.[5–7] The magnetic and magnetotransport properties of granular bimetallic systems (containing nearly superparamagnetic particles of a magnetic transition metal embedded into a metallic, nonmagnetic matrix) have been extensively studied;[8,9] more recently, bulk core-shell systems (compacted nanopowders of one transition metal surrounded by an oxidized shell) have been examined.[10] In these cases, the magnetic inhomogeneity on the nanometric scale is intimately related to a chemical inhomogeneity, with definite boundaries between adjacent chemical (and magnetic) phases. A natural extension is provided by magnetic systems in which the magnetic inhomogeneity on the nanometric scale is no longer related to chemical effects, and comes instead from magnetic frustration effects originated by competing interactions. In this paper, we address the case of ultra-short-range magnetic inhomogeneities in chemically homogeneous, concentrated systems such as mictomagnets and frustrated ferromagnets. These systems have often been depicted in a more sketchy way than spin glasses,[11] because of the intrinsic difficulty of providing an accurate theoretical description of the equilibrium spin arrangement; on the experimental side, magnetic measurements often offer as evidence a mixture of spin-glass and ferromagnetic features [such as the simultaneous presence of nonsaturating magnetization behavior up to very large fields,[12] and huge, steep magnetization changes at lower fields,[13,14] as well as evidence for irreversible effects and slow dynamics at all temperatures below T_C (Ref. 15)]. Getting a clear picture of concentrated disordered magnets is made difficult by the absence of independent experimental information to complement pure magnetic measurements, which hardly provide by themselves an unambiguous picture of the magnetic equilibrium state in a frustrated system. In Sec. II, we summarize the most recent magnetic and magnetotransport data obtained on disordered magnetic systems such as $Au_{100-x}Fe_x$ ($x=20$, 30) and $Cu_{60}Fe_{20}Ni_{20}$, evidencing the features common to all materials. A model is introduced in Sec. III to extract information on magnetic disorder from magnetoresistance data. Specific applications of the model are discussed in Sec. IV.

II. SUMMARY OF THE EXPERIMENTAL RESULTS

Rapidly solidified $Au_{80}Fe_{20}$, $Au_{70}Fe_{30}$, and $Cu_{60}Fe_{20}Ni_{20}$ alloys were submitted to full structural and magnetic characterization. Experimental details can be found in previous papers;[13,16,17] their common features are highlighted here:

(i) The considered alloys are nearly ideal solid solutions, at least in the as-quenched condition.[18,19]

(ii) In all studied systems there is clear evidence for a frustrated magnetic phase below the Curie temperature. In $Au_{80}Fe_{20}$, the spin arrangement has been defined as cluster

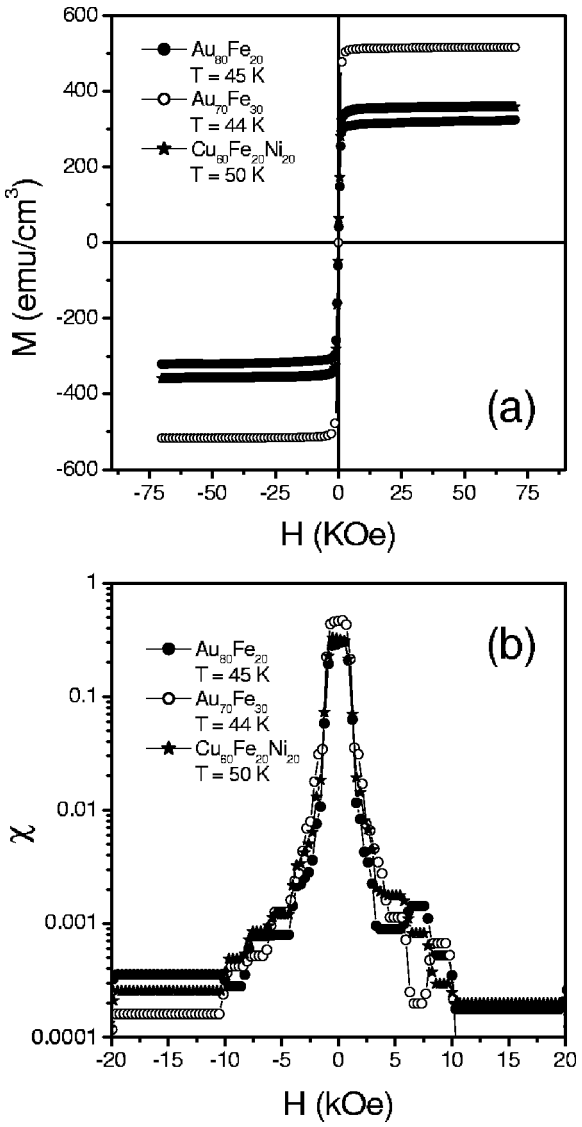

FIG. 1. (a) Typical magnetization curves of the studied alloys; (b) numerical field derivatives of the previous curves.

glass or mictomagnetic,[17,20] while $Au_{70}Fe_{30}$ and $Cu_{60}Fe_{20}Ni_{20}$ exhibit more definite ferromagnetic features. In all systems, magnetic and magnetotransport measurements point to the existence of a single magnetically ordered phase from 2 K to T_C.

(iii) Well below T_C, all isothermal magnetization curves exhibit no significant magnetic hysteresis and a two-step magnetization process, composed of a magnetization jump at low fields (typically for $H<2\times10^3$ Oe) followed by a very slow approach to saturation at high fields; no real saturation is observed up to 70 kOe; an example is shown in Fig. 1, where the magnetization and its numerical field derivative are plotted for the three alloys at about the same temperature.

(iv) All systems follow a simple paramagnetic behavior above T_C, according to a Curie-Weiss law with high effective moments,[17] indicating the presence of magnetic clusters even in the disordered phase. Typical values of the magnetic properties of interest are reported in Table I for all considered alloys.

TABLE I. Typical values of the magnetic quantities of interest. T_C: paramagnetic Curie temperature; μ_{eff}: effective moment per magnetic atom; T_{max}: temperature of maximum high-field magnetic permeability; H_W: Weiss field, estimated from T_C.

Alloy	T_C (K)	$\mu_{eff}(\mu_B)$	T_{max} (K)	H_W (Oe)
$Au_{80}Fe_{20}$	290	4.83	205	6.5×10^7
$Au_{70}Fe_{30}$	415	7.80	415	9.3×10^7
$Cu_{60}Fe_{20}Ni_{20}$	625	4.04	625	14.0×10^7

(v) All systems exhibit a negative magnetoresistance, essentially isotropic, whose values lie between a minimum of 2% for $Au_{70}Fe_{30}$ at $T=2$ K and a maximum of 17% for $Au_{80}Fe_{20}$ at $T=2$ K (always in the interval 0–70 kOe).[13] The dependence of MR on the reduced magnetization is far from quadratic, with an exception made for very high fields. A common aspect of these systems in their ordered phases is the boxlike shape assumed by the MR vs M/M_{sat} curves, and shown in Fig. 2(b). A continuous change from a boxlike to parabolic shape has been observed in $Au_{80}Fe_{20}$ corresponding with T_C.[13] The parabolic dependence observed in the paramagnetic phase[16] indicates that the magnetoresistance has the same origin as the GMR observed in bimetallic, nanogranular alloys, although here the scattering centers are single paramagnetic atoms or very small clusters of spins instead of being superparamagnetic particles.[16] The term proximity magnetoresistance[13] (PMR) indicates that the effect originates from spin-dependent electron scattering at the boundaries between coherence regions, which are no longer separated by a nonmagnetic phase as in granular alloys. PMR data are plotted as functions of both H and of M/M_{sat} in Fig. 2 for all alloys at about the same temperature. Detailed information on the equilibrium spin patterns is extracted from the PMR vs M/M_{sat} curves, according to a procedure described in the following section.

III. MAGNETIC CORRELATION LENGTH

Let us start with the relationship between electrical resistivity and the local direction of the magnetization vector in a magnetic material characterized by short-range magnetic order at equilibrium well below the ordering temperature (bulk frustrated magnet). Spin-dependent electron scattering is an essentially local phenomenon, which takes place at a given magnetic atom. The effects of scattering events on a macroscopic scale may be described through classical or semiclassical approaches, as is often done in the literature.[21,22] In principle, magnetic frustration at a local level, i.e., inherent disorder in the equilibrium spin directions down to the interatomic distance, may give rise to two types of effects on electron propagation: (i) an increase of resistivity by effect of the magnetic disorder, and (ii) a spatial dependence of the magnetic scattering cross section itself, by effect of the different pattern of the magnetic electron clouds existing in proximity to each magnetic scatterer. The latter effect will be disregarded in this paper; it is assumed here that the dominant effect of magnetic disorder is to add an extra contribution to the overall mean-free-path reduction, exactly as in

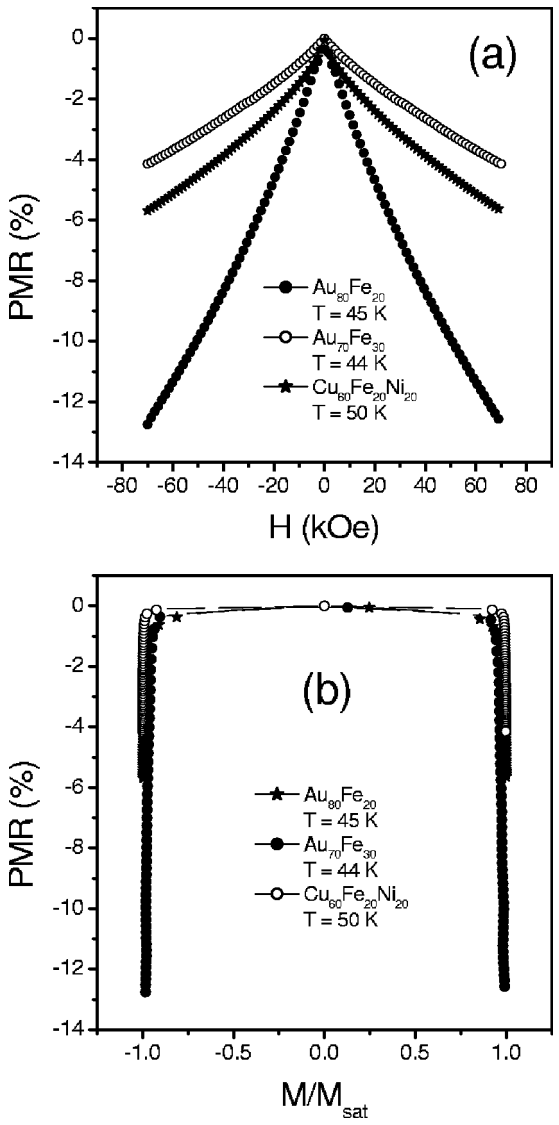

FIG. 2. Typical PMR curves of the studied alloys (a) plotted as functions of H and (b) plotted as functions of the reduced magnetization $\langle u\rangle = M/M_{sat}$.

superparamagnetic granular systems, where the same assumption is generally considered to hold.[8] The similarity between frustrated ferromagnets (exhibiting a static spin disorder) and superparamagnets (exhibiting a dynamical spin disorder) is strengthened considering that the electron time of flight between any two scatterers is very short compared with the lattice-lattice and spin-lattice relaxation times, so that electrons interact with an essentially static environment even in the case of spin fluctuations induced by thermal effects.[23]

The electrical resistance of a system where the magnetic scattering is not negligible may be simply written as[24]

$$R = R_0 - \alpha\langle \cos\theta_{ij}\rangle_\lambda , \tag{1}$$

where R_0 represents all nonmagnetic contributions to R, α is a quantity independent of the magnetic field, and θ_{ij} is the angle between the (instantaneous) direction of the atomic magnetic moment μ_i on the ith atom and that of the corresponding moment on the jth atom; the angular parentheses indicate an average over the material. The average is to be performed over all (i,j) pairs whose distance r_{ij} is of the order of magnitude of the electron mfp λ. The angle between instantaneous directions of μ_i and μ_j may be written in terms of a colatitude θ_i and of an azimuth ϕ_i, having introduced a fixed reference frame whose z axis is the direction of the external magnetic field. Using straightforward trigonometric relations, and factorizing the averages over colatitude and azimuth, one gets

$$\langle \cos\theta_{ij}\rangle = \langle \cos\theta_i \cos\theta_j\rangle + \langle \sin\theta_i \sin\theta_j\rangle \times \langle \cos(\phi_i - \phi_j)\rangle . \tag{2}$$

In the examined magnetic systems, it is assumed that a correlation exists between the directions of any two neighboring spins, and that this correlation monotonically decreases with increasing r_{ij}:

$$\langle \cos(\phi_i - \phi_j)\rangle = e^{(-r_{ij}/R_\phi)}, \tag{3}$$

$$\langle \cos\theta_i \cos\theta_j\rangle = (\langle \cos^2\theta\rangle - \langle \cos\theta\rangle^2) e^{(-r_{ij}/R_\theta)} + \langle \cos\theta\rangle^2, \tag{4}$$

$$\langle \sin\theta_i \sin\theta j\rangle = \langle \sin^2\theta\rangle e^{(-r_{ij}/R_\theta)}, \tag{5}$$

where R_θ and R_ϕ are two correlation ranges for colatitude and azimuth correlation, respectively. The two correlation lengths, R_θ and R_ϕ, may be considered as substantially equal in bulk frustrated magnets. This assumption does not hold for correlated paramagnetic or superparamagnetic particles,[9] where the mechanisms determining longitudinal and transverse spin correlations and their breakdown are different;[23] however, in the present case, where a *static* disorder takes the place of the dynamical disorder produced by temperature, this assumption is reasonable because the local canting of spins is no longer related to two different channels of spin relaxation. Instead it is related to the presence of a randomly oriented local anisotropy axis, determined by competition between magnetic interactions. Let us explicitly assume $R_\theta = R_\phi = R_m$. In this case, the average value appearing in Eq. (2) may be written as

$$\langle \cos\theta_{ij}\rangle_\lambda = m^2 + (\langle u^2\rangle - \langle u\rangle^2) e^{(-\lambda/R_m)} + (1 - \langle u^2\rangle) e^{(-2\lambda/R_m)}, \tag{6}$$

where $u = \cos\theta$, $\langle u\rangle$ corresponds to the reduced magnetization M/M_{sat}, and the condition $r_{ij} = \lambda$ has been explicitly introduced.

The correlation length must vanish for high fields;[25] as a consequence, the electrical resistance must depend on the square of the reduced magnetization for sufficiently high values of the magnetic field. Such a result is indeed observed in all examined systems (an example is shown in Fig. 3). The parabolic law interpolating the experimental resistance at high fields is

$$R^* = R_0 - \alpha\langle u\rangle^2 \tag{7}$$

so that it is possible to write

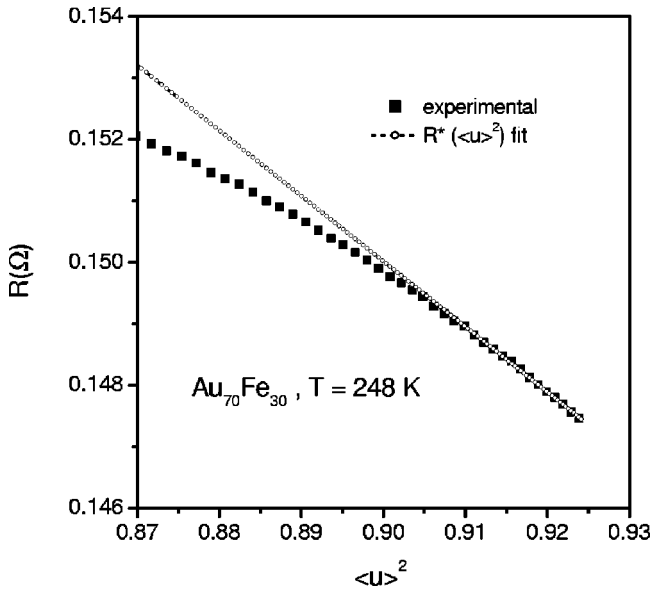

FIG. 3. Experimental dependence of electrical resistance R on $\langle u\rangle^2$ near magnetic saturation.

$$R^*-R=\alpha[(\langle u^2\rangle-\langle u\rangle^2)e^{(-\lambda/R_m)}+(1-\langle u^2\rangle)e^{(-2\lambda/R_m)}]. \tag{8}$$

Equation (8) is a simple algebraic equation of the second degree in $x=e^{(-\lambda/R_m)}$. Introducing the field-dependent quantities $A=1-\langle u^2\rangle$; $B=(\langle u^2\rangle-\langle u\rangle^2)$; $C=(R^*-R)/\alpha$ it becomes

$$Ax^2+Bx-C=0. \tag{9}$$

The coefficients *A*, *B*, and *C* can be determined from experiment. The quantity *C* is directly obtained by interpolating the experimental resistance data at high fields through Eq. (7). In order to obtain the quantity $\langle u^2\rangle$ entering the coefficients A and B, a simplified picture of the magnetization mechanism in frustrated magnets may be used. It is supposed here that the distribution at equilibrium of the local directions of magnetization under a given magnetic field may be represented by the spherical random-walk function introduced by Zener[26] and defined by

$$\Phi_{RW}(\theta,\tau)=\frac{1}{2\pi}\sum_{n=0}^{\infty}\frac{2n+1}{2}e^{-n(n+1)\tau}P_n(\cos\theta), \tag{10}$$

where θ is the angle between the local magnetization direction and the field direction, and τ is a field-dependent parameter ranging from zero to infinity, determining the spread of the distribution (Φ_{RW} reduces to a delta function for $\tau\to 0$, and becomes the constant 1/2 for $\tau\to\infty$). Both the reduced magnetization $\langle u\rangle$ and the relationship between $\langle u^2\rangle$ and $\langle u\rangle$ are easily obtained by exploiting the orthogonality of Legendre polynomials; as it turns out,

$$\langle u\rangle(H)=e^{-2\tau(H)},$$

$$\langle u^2\rangle=\frac{1}{3}+\frac{2}{3}\langle u\rangle^3. \tag{11}$$

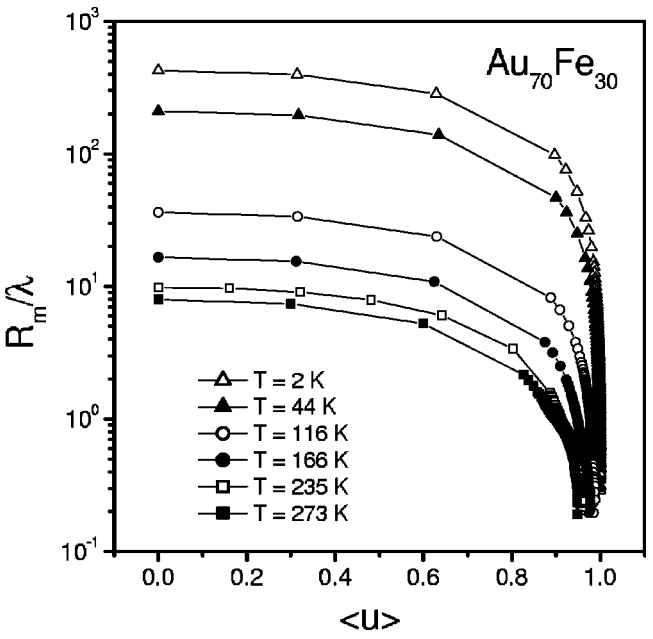

FIG. 4. R_m/λ vs $\langle u\rangle$ for $Au_{70}Fe_{30}$ at different temperatures.

The quantity R_m/λ is easily obtained from Eq. (9) as

$$R_m/\lambda=\frac{1}{\ln 1/x}. \tag{12}$$

At fixed *T*, this quantity is a function of *H*, monotonically decreasing from the starting value $R_m(0)/\lambda$ to zero. Examples are given in Figs. 4–6 for all considered systems at selected temperatures; the best way for having all results displayed on a single graph for each alloy is to use a logarithmic scale for the vertical axis, and to keep the reduced magnetization $\langle u\rangle$ as the independent variable. Fluctuations

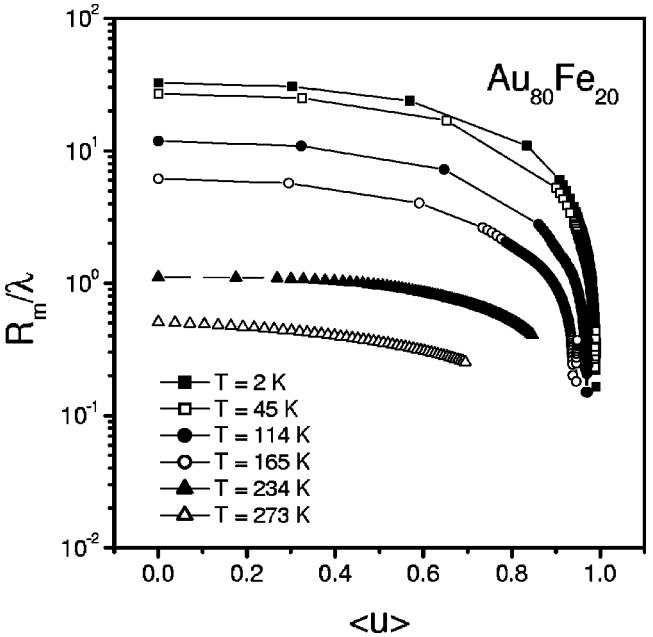

FIG. 5. R_m/λ vs $\langle u\rangle$ for $Au_{80}Fe_{20}$ at different temperatures.

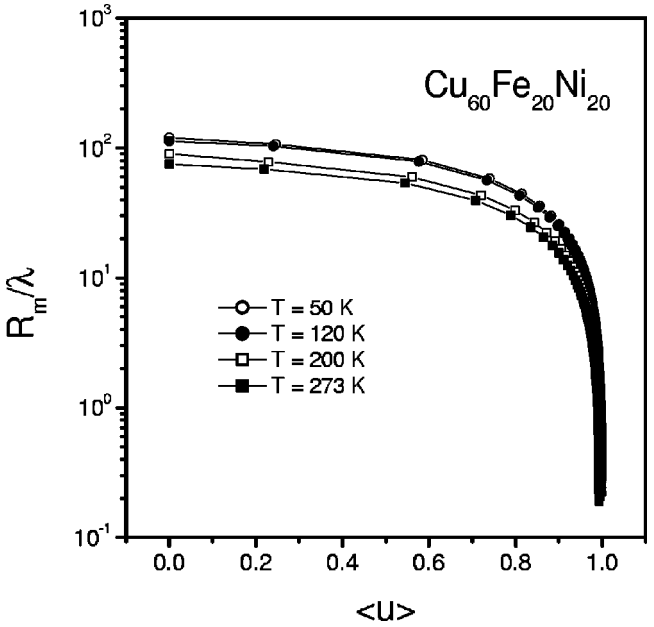

FIG. 6. R_m/λ vs $\langle u \rangle$ for $Cu_{60}Fe_{20}Ni_{20}$ at different temperatures.

at high fields are unavoidable by-products of the procedure, which involves the determination of the logarithm of a quantity close to zero. More physical insight will be obtained plotting the curves as functions of *H*, as discussed in Sec. IV C. Generally speaking, $R_m(0)/\lambda$ is a decreasing function of temperature, although in $Cu_{60}Fe_{20}Ni_{20}$ such a dependence is significantly weaker than in the other two cases. This is mainly related to the different Curie temperatures of the three alloys, as discussed in Sec. IV B. As observed, R_m/λ values comparable to or lower than unity are found: (i) at large $\langle u \rangle$ values, in all systems; (ii) over the entire $\langle u \rangle$ range, in the $Au_{80}Fe_{20}$ alloy at the highest temperatures. Finally, it should be noted that the present results are not substantially affected by the choice of the relationship between $\langle u^2 \rangle$ and $\langle u \rangle$; in fact, it has been checked that any other physically meaningful choice brings about but minor consequences on the R_m/λ curves. In particular, the maximum value $[R_m(0)/\lambda]$ and the high-field limit (i.e., zero) remain exactly the same, while the R_m/λ vs $\langle u \rangle$ curve is only weakly modified in shape, and its concavity does not change sign.

IV. APPLICATIONS

A. Effect of R_m/λ on the magnetoresistance

The effect of the value of R_m/λ on the shape of the experimental magnetoresistance curve can be easily understood. Let us consider the case $R_m(0)/\lambda \gg 1$, corresponding to a very large magnetic correlation length at zero field. This case corresponds to the boxlike behavior of the magnetoresistance plotted vs $\langle u \rangle$, and characterized by an exceedingly flat central region and by a dramatic drop of the electrical resistance *R* when $|\langle u \rangle|$ approaches unity [see Fig. 2(b)]. The central region corresponds to large coherence regions, whose widths are much larger than λ. In these conditions, any pair of adjacent scattering centers, at a distance λ apart, are always inside the same coherence region (excluding border effects at boundaries), so that the field does not appreciably affect the angle θ_{ij}, and the resistance stays constant even in the presence of large variations of $\langle u \rangle$. On the contrary, the region of the $R(\langle u \rangle)$ curve close to $|\langle u \rangle| = 1$ corresponds to a strong reduction of the term R_m/λ, which is dropping to zero, so that spins at a distance λ apart become statistically unfrozen, and the MR begins to be observed. In most cases, the same region corresponds to a small residual increment of $\langle u \rangle$, so that the MR curve appears as typically squeezed towards $|\langle u \rangle| = 1$. The variation of the electrical resistance *R* at high fields implies that a significant canting of spins occurs over distances of the order of the electron mfp. This gives additional support to our picture of the coherence regions as zones where the spin alignment is initially far from being perfect. Small values of $R_m(0)/\lambda$ (i.e., not very large with respect to unity) imply instead a nearly parabolic MR behavior with $\langle u \rangle$ (somewhat reminiscent of the flat-top parabolas found in superparamagnetic granular systems[9]). Two experimental MR curves corresponding to these two limiting cases are shown in Fig. 7.

B. Correlation length: Absolute values

Absolute values of $R_m(0)$ are immediately calculated from $R_m(0)/\lambda$ using the electron mean free path obtained from zero-field electrical resistance measurements. A variety of $R_m(0)$ values is found, depending on the alloy composition and temperature. Generally speaking, $R_m(0)$ is a decreasing function of temperature, the smallest slope corresponding to $Cu_{60}Fe_{20}Ni_{20}$, whose Curie temperature is the highest (Table I). The $R_m(0)$ data for the three studied alloys are reported as functions of the reduced temperature T/T_C in Fig. 8, to emphasize the effect of the increasing loss of magnetic order on the maximum correlation length. Although all curves exhibit a similar trend, no truly universal behavior is observed, reflecting the fact that the material composition has some impact (not accounted for by the model) on the temperature dependence of $R_m(0)$. This quantity attains the value of about one micrometer in $Au_{70}Fe_{30}$ at very low *T*. Such a value is compatible with the picture of this alloy as a long-range ferromagnet at low temperatures, as independently indicated by dc susceptibility measurements.[13] When $T/T_C \rightarrow 1$, the correlation length $R_m(0)$ of $Au_{80}Fe_{20}$ approaches the horizontal line which indicates the average nearest-neighbor distance in the same alloy, as deduced from x-ray diffraction.[19] Above about 280 K all spins become statistically independent; such a result is in agreement with the existing information on both the paramagnetic Curie temperature and the broad order-disorder transition of this alloy, obtained through dc susceptibility measurements at low and high fields, respectively (Table I).

A somewhat complementary view is provided by the analysis of the parameter $\Pi_a = \langle \cos \theta_{ij} \rangle_\lambda$ of Eq. (1), which is a measure of the degree of parallelism among spins within a sphere of radius λ. In particular, the limits $\Pi_a = 0$ and $\Pi_a = 1$ are associated with completely random spin directions and perfect spin alignment, respectively. The parameter Π_a is easily obtained as $[R^*(0) - R(0)]/\alpha$ from the procedure of Sec. III, and is plotted as a function of temperature in Fig.

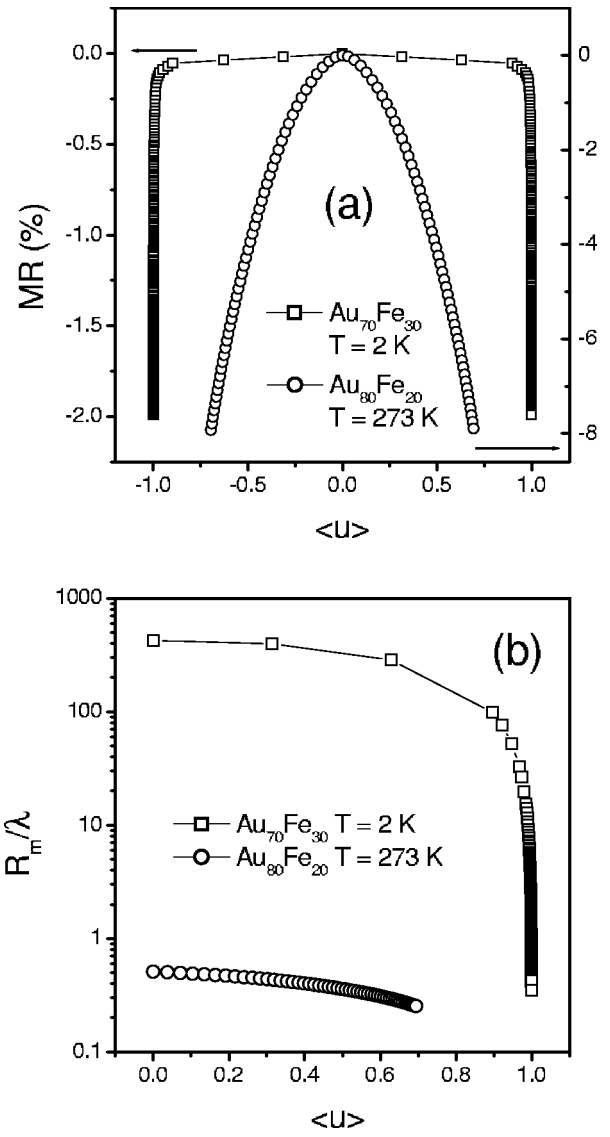

FIG. 7. (a) Limiting cases of the observed magnetoresistance curves (parabolic and boxlike behavior); (b) corresponding R_m/λ vs $\langle u \rangle$ curves.

9. Once again, the most perfect alignment over the distance λ is found in $Cu_{60}Fe_{20}Ni_{20}$; the same condition is attained by $Au_{70}Fe_{30}$ at the lowest temperatures; in $Au_{80}Fe_{20}$ the alignment is rapidly lost with increasing T, and almost random spin directions are observed in correspondence of the paramagnetic transition, as expected. Remarkable properties of frustrated systems emerge when the parameter Π_a is plotted as a function of the ratio $R_m(0)/\lambda$. Figure 10 clearly shows that $\Pi_a \rightarrow 0$ when $R_m(0)/\lambda$ becomes equal to or smaller than 1 (corresponding to the case of a perfect paramagnet). The interesting aspects of Fig. 10 are (i) the degree of local spin parallelism (defined within a sphere of radius λ, which is always of the order of magnitude of the nearest-neighbor distance) is determined by the radius of the sphere of coherence, which usually is much larger; therefore local and medium-ranged properties of the spin pattern are intimately entangled in these frustrated systems; (ii) all points fall on a single curve, independently of the alloy type and composition: this result indicates that the relation between local alignment and coherence length may be a very general property of bulk frustrated magnets. Finally, it can be observed that a significant spin misalignment on the scale of λ ($\Pi_a \approx 0.9$) exists even in considerably large coherence regions [$R_m(0)/\lambda \approx 14$, corresponding in these alloys to a volume containing approximately 1×10^6 correlated spins]. This result is not surprising, because the tendency towards spin parallelism is always in competition with local anisotropy fields originating from the random magnetic interactions, so that small-scale frustration survives to some extent in the form of

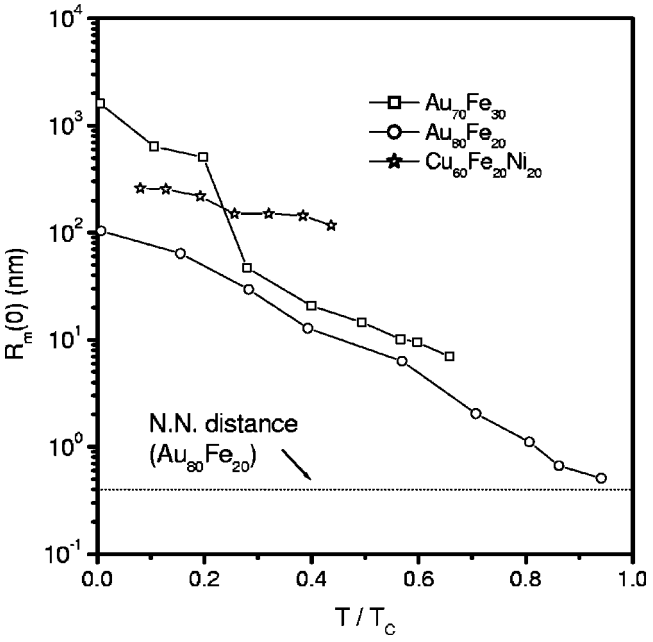

FIG. 8. Zero-field magnetic correlation length $R_m(0)$ as a function of reduced temperature T/T_C.

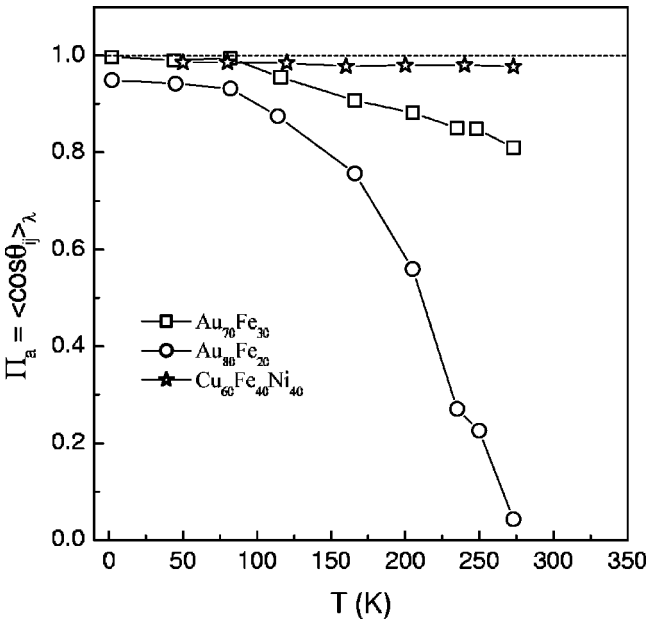

FIG. 9. Local alignment parameter Π_a as a function of temperature for the studied alloys (see text for details).

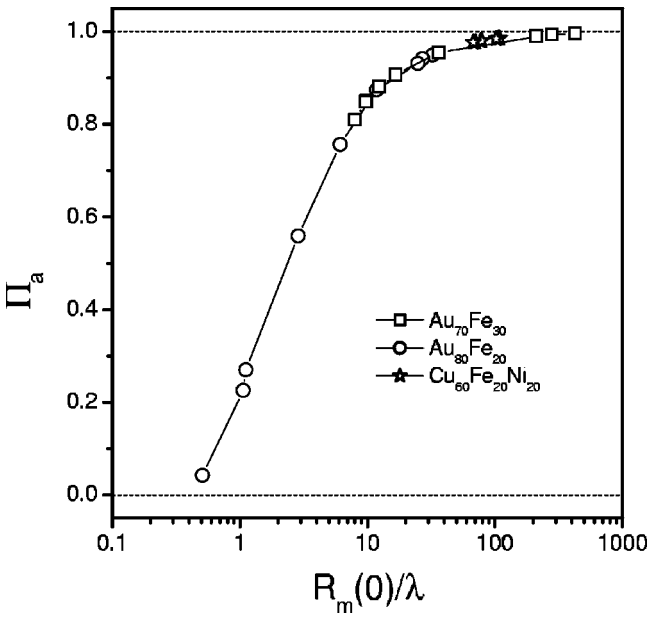

FIG. 10. Local alignment parameter Π_a as a function of $R_m(0)/\lambda$ for the studied alloys.

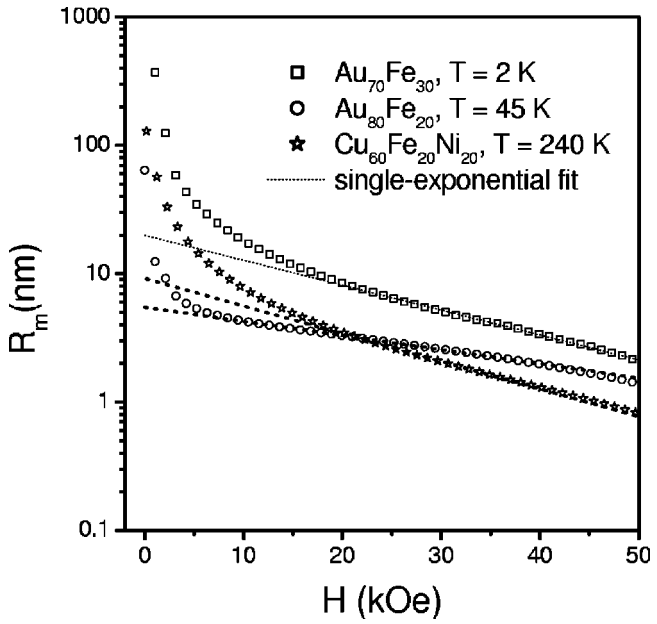

FIG. 11. Semilogarithmic plots of R_m vs H, evidencing the high-field exponential behavior of the magnetic correlation length.

a misalignment of spins even in large-scale ''blocks'' of correlated spins. Figure 10 shows that the spin misalignment gradually disappears when the correlation length is further increased; it can be assumed as negligible only for correlated volumes containing about 1×10^{10} spins (a magnetic domain in a bulk metallic ferromagnet such as monocrystalline Fe may contain $10^{20}-10^{22}$ aligned spins).

C. Functional dependence of $R_m(H)$: The correlation field

The analytical expression for the correlation length R_m for all H values cannot be obtained from the present approach. In fact, the functional dependence at low H values is affected by the details of the initial magnetization process, which can be rather complex in a frustrated magnet. It should be reiterated that the random correlation field acting on each spin is a mere representation of the true interaction among spins, a genuine many-body effect. However, at high fields $R_m(H)$ should asymptotically behave as an exponential function of H:

$$R_m(H)\propto e^{-H/H_{corr}}, \tag{13}$$

where H_{corr} may be taken as a figure of the rms correlation field: when $H\gg H_{corr}$, the width of the coherence regions is significantly less than λ. The $R_m(H)$ curves obtained through our procedure suggest that this can indeed be the case, although the observation spans one decade only. In the restricted range of R_m values explored, a single-exponential behavior of $R_m(H)$ is observed at high fields, as shown in Fig. 11 for the examined systems at three selected temperatures. In this way, an estimate of H_{corr} can be obtained for all bulk frustrated magnets under study. These values are reported in Table II; it should be noted that they are much larger than dipolar fields found in other granular systems,[27] as expected, but still well below the Curie-Weiss field of these bulk ferromagnets, as estimated from their Curie temperatures (see Table I).

V. CONCLUDING REMARKS

The proposed approach provides a simple, effective way to describe the magnetoresistance properties of concentrated, bulk magnetic systems containing frustrated spins. These materials may be considered as nanoscale systems because of the ultrashort magnetic coherence length; they somewhat fill the gap between dilute frustrated systems (spin glasses) and standard ferromagnets. Magnetoresistance effects in these systems have been straightforwardly related to the nanoscopic coherence length. The present results allow one to interpret a variety of experimental MR data in terms of one parameter, the magnetic coherence length. In particular, the typical boxlike shape exhibited by the MR when plotted as a function of M/M_{sat} is interpreted in terms of a magnetic correlation range which is much larger than the electron mfp λ when $H=0$, and reduces to less than λ for sufficiently high fields. The high-magnetization ''tails'' of the boxlike MR asymptotically follow a $\langle u\rangle^2$ dependence, in agreement with the expected behavior of a spin-spin correlation, which must disappear at high fields. The characteristically flattened central region of boxlike MR curves does not imply the perfect alignment of spins over distances of the order of λ;

TABLE II. Typical values of H_{corr} (in Oe) obtained using Eq. (13).

T (K)	$Au_{70}Fe_{30}$	$Au_{80}Fe_{20}$	$Cu_{60}Fe_{20}Ni_{20}$
50	2.3×10^5	3.4×10^5	3.3×10^5
160	4.9×10^5	4.0×10^5	2.3×10^5
250	5.0×10^5	5.8×10^5	2.0×10^5

instead it means that any angle between canted spins is very stable against external disturbances: the correlation manifests itself in a coherent spin rotation under the magnetic field, with a negligible MR effect. This angular correlation actually originates from a collective interaction, involving many adjacent spins; it can be represented by the random anisotropy field, or correlation field, introduced in Sec. IV. With increasing H above H_{corr}, the angular correlation is expected to decrease, although the overall alignment among spins increases. The $H=0$ state of these materials corresponds to a significant canting of neighboring spins; the degradation of this canted state under high fields gives rise to the strong MR effect which emerges in the high-magnetization region of the boxlike curves. The abrupt change of derivative characterizing the experimental MR vs M/M_{sat} curves (and justifying the name of ''boxlike'' given to this type of curve) is connected to the exponential decrease of the magnetic correlation range at sufficiently high fields, resulting in an enhanced MR effect, which appears as squeezed towards $|M/M_{sat}|=1$ when the MR is plotted against reduced magnetization. The local alignment parameter defined in Sec. IV provides a quantitative estimate of the initial degree of spin canting.

The continuous transition from a boxlike to a fully parabolic behavior of MR vs M/M_{sat}, observed, for instance, in $Au_{80}Fe_{20}$ (Ref. 13) when the temperature is increased from 2 K to 300 K, may be coherently related to the reduction of the zero-field magnetic coherence length with T. In this case, the magnetic coherence length becomes vanishingly small close to the paramagnetic transition, with no significant critical-point anomalies.

In conclusion, the magnetoresistance properties of the considered frustrated magnets can be fully understood in terms of concepts derived from those introduced in the description of the giant magnetoresistance in superparamagnetic granular systems. Relating the MR effects to the nanoscale magnetic properties of bulk frustrated magnets is a particularly effective way to get a unified picture of this class of systems.

[1] M.N. Baibich, J.M. Broto, A. Fert, F. Nguyen van Dau, F. Petroff, P. Etienne, G. Creuzet, A. Friederich, and J. Chazelas, Phys. Rev. Lett. **61**, 2472 (1988).

[2] A. Fert and P. Bruno, in *Ultrathin Magnetic Structures II* (Springer-Verlag, Berlin, 1987), p. 82.

[3] H. Hauser and M. Tondra, in *Magnetic Sensors and Magnetometers*, edited by P. Ripka (Artech House, Boston, 2001), p. 129.

[4] S. Zhang and P.M. Levy, J. Appl. Phys. **73**, 5315 (1993).

[5] Z. Sefrioui, J.L. Menendez, E. Navarro, A. Cebollada, F. Briones, P. Crespo, and A. Hernando, Phys. Rev. B **64**, 224431 (2001).

[6] L. Dimesso and H. Hahn, J. Appl. Phys. **84**, 953 (1998).

[7] B. Heinrich and J.A.C. Bland, in *Ultrathin Magnetic Structures I* (Springer-Verlag, Berlin, 1987), p. 1.

[8] A.E. Berkowitz, J.R. Mitchell, M.J. Carey, A.P. Young, S. Zhang, F.E. Spada, F.T. Parker, A. Hütten, and G. Thomas, Phys. Rev. Lett. **68**, 3745 (1992); J.Q. Xiao, J.S. Jiang, and C.L. Chien, *ibid.* **68**, 3749 (1992).

[9] P. Allia, M. Knobel, P. Tiberto, and F. Vinai, Phys. Rev. B **52**, 15 398 (1995).

[10] L. Savini, E. Bonetti, L. Del Bianco, L. Pasquini, S. Signoretti, P. Allia, M. Coisson, J. Moya, V. Selvaggini, P. Tiberto, and F. Vinai, J. Appl. Phys. **91**, 8593 (2001).

[11] See for instance, J.A. Mydosh and G.J. Nieuwenhuys, in *Ferromagnetic Materials I*, edited by E.P. Wohlfarth (North-Holland, Amsterdam, 1980), p. 79.

[12] L. Del Bianco, E. Bonetti, D. Fiorani, D. Rinaldi, R. Caciuffo, and A. Hernando, J. Magn. Magn. Mater. **226**, 1478 (2001).

[13] P. Allia, M. Coisson, G.F. Durin, J. Moya, V. Selvaggini, P. Tiberto, and F. Vinai, J. Appl. Phys. **91**, 5936 (2002).

[14] P. Allia, M. Coisson, J. Moya, V. Selvaggini, P. Tiberto, F. Vinai, and E. Bosco, Mater. Sci. Eng., A (to be published).

[15] Anindita Ray, R. Ranganathan, and C. Bansal, Phys. Rev. B **56**, 6073 (1997).

[16] P. Allia, M. Coisson, V. Selvaggini, P. Tiberto, and F. Vinai, Phys. Rev. B **63**, 180404 (2001).

[17] P. Allia, M. Coisson, J. Moya, V. Selvaggini, P. Tiberto, and F. Vinai, Phys. Status Solidi A **189**, 321 (2002).

[18] M. Baricco, E. Bosco, G. Acconciaioco, P. Rizzi, and M. Coisson, Mater. Sci. Eng., A (to be published).

[19] E. Bosco, P. Rizzi, and M. Baricco, Mater. Sci. Eng., A (to be published).

[20] P.A. Beck, Phys. Rev. B **28**, 2516 (1983).

[21] R.E. Camley and J. Barnas, Phys. Rev. Lett. **63**, 664 (1989).

[22] A. Fert and P. Bruno, in *Ultrathin Magnetic Structures II* (Ref. 1), p. 98.

[23] P. Allia, P. Tiberto, and F. Vinai, J. Appl. Phys. **81**, 4599 (1997).

[24] J.Q. Xiao, J.S. Jiang, and C.L. Chien, Phys. Rev. Lett. **68**, 3749 (1992).

[25] A. Herpin, in *Théorie du Magnétisme* (Presses Universitaires de France, Paris, 1968), p. 294.

[26] C. Zener, Phys. Rev. **96**, 1335 (1954).

[27] P. Allia, M. Coisson, M. Knobel, P. Tiberto, and F. Vinai, Phys. Rev. B **60**, 12 207 (1999).